

Competition between Ekman Plumes and Vortex Condensates in Rapidly Rotating Thermal Convection

Andrés J. Aguirre Guzmán¹,[✉] Matteo Madonia¹,[✉] Jonathan S. Cheng,^{1,*} Rodolfo Ostilla-Mónico²,[✉]
Herman J. H. Clercx¹,[✉] and Rudie P. J. Kunnen^{1,†}

¹*Fluids and Flows group, Department of Applied Physics and J. M. Burgers Centre for Fluid Dynamics, Eindhoven University of Technology, P.O. Box 513, 5600 MB Eindhoven, Netherlands*

²*Department of Mechanical Engineering, University of Houston, Houston, Texas 77004, USA*

 (Received 7 April 2020; revised 15 July 2020; accepted 23 October 2020; published 20 November 2020)

We perform direct numerical simulations of rotating Rayleigh-Bénard convection (RRBC) of fluids with low ($Pr = 0.1$) and high ($Pr \approx 5$) Prandtl numbers in a horizontally periodic layer with no-slip bottom and top boundaries. No-slip boundaries are known to actively promote the formation of plumelike vertical disturbances, through so-called Ekman pumping, that control the ambient flow at sufficiently high rotation rates. At both Prandtl numbers, we demonstrate the presence of competing large-scale vortices (LSVs) in the bulk. Strong buoyant forcing and rotation foster the quasi-two-dimensional turbulent state of the flow that leads to the upscale transfer of kinetic energy that forms the domain-filling LSV condensate. The Ekman plumes from the boundary layers are sheared apart by the large-scale flow, yet we find that their energy feeds the upscale transfer. Our results of RRBC simulations substantiate the emergence of large-scale flows in nature regardless of the specific details of the boundary conditions.

DOI: [10.1103/PhysRevLett.125.214501](https://doi.org/10.1103/PhysRevLett.125.214501)

In fluid dynamics, viscous boundary layers (BLs) adjacent to no-slip surfaces are frictional regions that, despite being relatively thin, can greatly affect the dynamics of the ambient flow. In particular, the so-called Ekman BL in rapidly rotating flows [1] actively enhances vertical velocities far beyond the BL region through Ekman pumping. Likewise, Ekman pumping boosts convective instabilities of the thermal BL in buoyancy-driven flows, a highly relevant problem to many geophysical and astrophysical systems. These flows span the domain height at sufficiently strong rotation [2–6]. When rotation is much weaker than thermal forcing, however, plumes emerging from the BL organize into a large-scale circulation (LSC) with shearing that ironically sweeps away the plumes formed by the BL [7,8].

For a surface with stress-free boundary condition, the buoyancy-driven flow fed by the thermal BL is no longer enhanced by Ekman pumping. The thermal plumes are then too weak to affect the ambient flow, which becomes more prone to turbulence under strong thermal forcing. At sufficiently strong forcing and rapid rotation, vertical velocities are largely suppressed, and the resulting turbulent flow is quasi-two-dimensional (Q2D) [5,9–13]. The flow then mimics pure 2D turbulence with an inverse energy cascade [14,15]. The upscale energy transfer is eventually balanced by friction in finite-size domains or by imposed large-scale damping. Consequently, energy accumulates at large scales (spectral condensation) and large-scale vortices (LSVs; also called vortex condensates) form [16–20]. However, the question is whether similar processes occur

for no-slip boundaries; can LSVs sweep away the (Ekman) plumes as the LSC does at low rotation rates?

Here, we demonstrate for the first time the presence of coherent, long-lived LSVs in rotationally constrained thermal convection despite Ekman pumping interaction from the BLs. We do so for fluids of different Prandtl number (defined below) pertinent to geophysical systems: low $Pr = 0.1$, relevant to liquid metals as in Earth's outer core, and high $Pr \approx 5$, water, popular in experiments and applicable to oceanic processes. We identify nonlocal energy transfer from smaller scales to the largest horizontal scale in the domain, while the Q2D turbulent bulk subdues significant disturbances from the BLs. Our novel observation of LSVs with no-slip walls paves the way to experimentally explore LSV growth in buoyancy-driven rotating turbulence, a process omnipresent in large-scale natural flows. We directly assess the effects of no-slip boundaries on vortex condensates in 3D anisotropic systems. So far, simulations have typically employed stress-free conditions. Recent convection simulations using parametrized Ekman pumping boundary conditions report upscale transfer of kinetic energy but no persistent LSVs form [21,22].

We consider rotating Rayleigh-Bénard convection (RRBC), the flow confined between parallel horizontal walls, heated from below and cooled from above, subject to background rotation. Three nondimensional parameters govern RRBC: the Rayleigh number $Ra = g\alpha\Delta H^3/(\nu\kappa)$ quantifies the intensity of buoyant forcing, the Ekman number $Ek = \nu/(2\Omega H^2)$ measures the (inverse) strength of rotation, and the Prandtl number $Pr = \nu/\kappa$ describes the

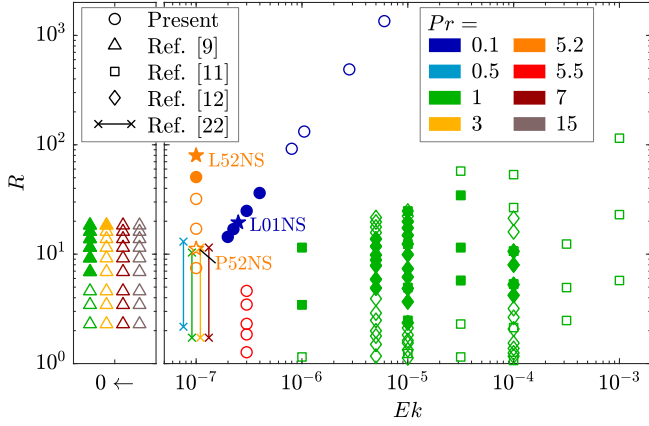


FIG. 1. Phase diagram of rotating convection. Present no-slip DNS; asymptotic ($Ek \rightarrow 0$) simulations, with stress-free [9] and parametrized Ekman-pumping boundaries [22]; stress-free DNS [11,12]. Filled symbols represent LSV states. Labeled stars are reference cases from the present study.

diffusive properties of the fluid. Here, g is gravitational acceleration, α , ν , and κ are, respectively, the kinematic viscosity, thermal diffusivity, and thermal expansion coefficient of the fluid, Δ and H the temperature difference and distance between bottom and top wall, respectively, and Ω the rotation rate. The critical Rayleigh number for onset of oscillatory convection ($Pr < 0.68$) is $Ra_c = 17.4(Ek/Pr)^{-4/3}$; for steady convection ($Pr \geq 0.68$) it is $Ra_c = 8.7Ek^{-4/3}$ [23,24]; $R \equiv Ra/Ra_c$ measures supercriticality.

We perform direct numerical simulations (DNSs) of the incompressible Boussinesq Navier-Stokes and heat equations [23], nondimensionalized by Δ , H and (free-fall) velocity $U_{ff} = \sqrt{g\alpha\Delta H}$, with no-slip boundaries at parameters displayed in Fig. 1 (circles). We employ second-order finite-difference discretizations [25] on a grid vertically denser near the walls to resolve the thinner (Ekman or thermal) BL with at least 10 points. At $Pr = 0.1$, the dimensions of the horizontally periodic computational domain are $10\ell_c^o \times 10\ell_c^o \times 1$, where $\ell_c^o = 2.4(Ek/Pr)^{1/3}$ is the horizontal length scale for onset of oscillatory convection [23,24]. Resolutions up to $1408 \times 1408 \times 1280$ points resolve the Kolmogorov length η_K , the smallest active flow length scale. For $Pr \approx 5$ the domain is $20\ell_c^s \times 20\ell_c^s \times 1$ [26], with $\ell_c^s = 2.4Ek^{1/3}$ the onset scale for steady convection [23,24]. A fine grid with up to $1536 \times 1536 \times 2048$ points resolves the temperature field down to the Batchelor length $\eta_B = \eta_K/Pr^{1/2}$, its smallest active length scale, and a coarser grid resolves the velocity field to η_K [25]. Three reference cases, indicated with stars (Fig. 1), are selected for further analysis: LSVs at $Pr = 0.1$, $R = 20$ (L01NS; L01SF is a corresponding stress-free run) and at $Pr = 5.2$, $R = 80$ (L52NS), and plumes at $Pr = 5.2$, $R = 11$ (P52NS).

In the bulk, the relative magnitude of root-mean-square (RMS) horizontal (u_{RMS}) and vertical (w_{RMS}) velocity

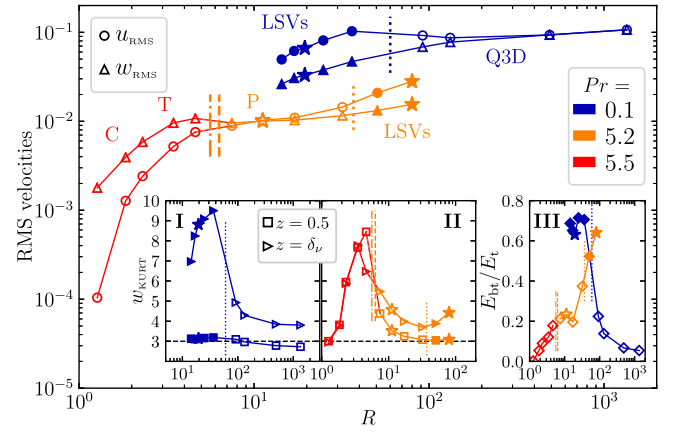


FIG. 2. RMS horizontal (u_{RMS}) and vertical (w_{RMS}) velocities at midheight ($z = 0.5$) versus R . Vertical dash-dotted and dashed lines indicate predicted transitions from cells (C)/convective Taylor columns (T) to plumes (P) [27,28]. Vertical dotted lines are our estimated transitions between plumes and LSVs (orange), and LSVs and Q3D (blue). Inset I and II: vertical-velocity kurtosis w_{KURT} at midheight (squares) and at the Ekman BL thickness ($z = \delta_\nu$; right triangles). Horizontal dashed lines at $w_{KURT} = 3$ indicate Gaussian kurtosis. Inset III: ratio of barotropic E_{bt} to total E_t kinetic energy. Filled symbols denote LSV cases.

exhibits significantly different behavior specific to the flow structure that, together with the vertical-velocity kurtosis (w_{KURT}), provides a generic way to distinguish the flow regimes identified in Ref. [9]. For cells (C) and convective Taylor columns (T) vertical velocities are stronger than horizontal, for plumes (P) [and quasi-3D (Q3D) turbulence at $Pr = 0.1$] they are comparable, while for LSVs horizontal velocities are larger (Fig. 2). Larger-than-Gaussian kurtosis, i.e., $w_{KURT} > 3$, indicates increased likelihood of strong vertical velocity fluctuations. Reference [9] reports $w_{KURT} > 3$ at midheight for cells, columns, and plumes, while in the so-called geostrophic turbulence state (where LSVs are observed) $w_{KURT} \approx 3$ as in homogeneous isotropic turbulence. Our midheight observations are the same (inset I and II).

LSV states are emphasized by the decomposition into 2D (vertically averaged) barotropic flow and 3D (depth-dependent) baroclinic convection [9–11]: $\mathbf{u} = \langle \mathbf{u} \rangle_z + \mathbf{u}'$, where $\langle \mathbf{u} \rangle_z = \int_0^1 \mathbf{u} dz$. The ratio of barotropic $E_{bt} = \frac{1}{2}(\langle u \rangle_z^2 + \langle v \rangle_z^2)$ to total $E_t = \frac{1}{2}(u^2 + v^2 + w^2)$ kinetic energy is largest for LSVs (inset III); the 2D flow dominates as is common in condensate vortices [9,20,29]. The large fraction of 2D kinetic energy, larger horizontal than vertical RMS velocity, and Gaussian bulk kurtosis are signatures of Q2D turbulence in the LSV flow state. Near the bottom at height $z = \delta_\nu$ (the Ekman BL thickness based on the u_{RMS} maxima) kurtosis follows the bulk trend for most of the R range, except for LSV states where it remains larger than 3. We hypothesize that deviations from Gaussianity are caused by the prevalence

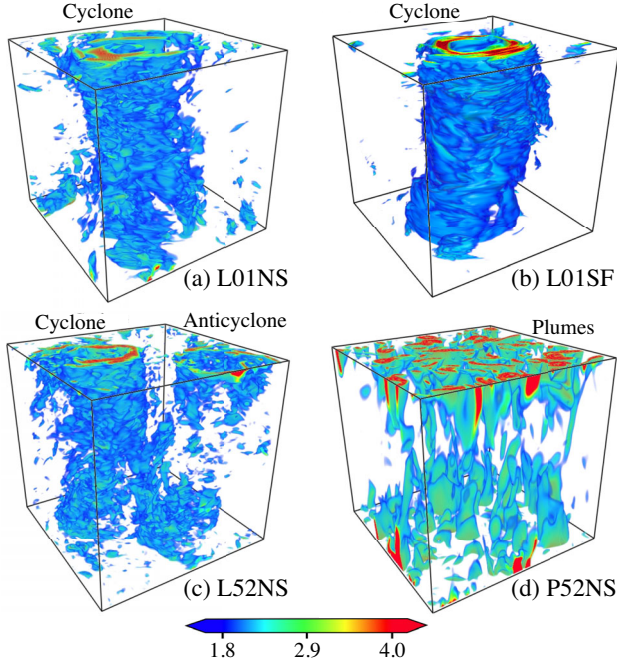


FIG. 3. Snapshots of horizontal kinetic energy $\frac{1}{2}(u^2 + v^2)$, scaled by volume-averaged total energy $\langle E_t \rangle_V$ for the reference cases (a) L01NS, (b) L01SF, (c) L52NS, and (d) P52NS. Actual domains are slender; their width-to-height ratio $\Gamma = W/H = \mathcal{O}(10^{-1})$. For clarity, they are stretched horizontally by a factor $1/\Gamma$.

of smaller-scale structures formed by Ekman pumping from the BLs, whose presence, remarkably, does not disrupt the LSVs. This will be addressed later.

Flow visualizations in Fig. 3 of the reference cases reveal for both L01NS and L01SF [panels (a) and (b)] one large-scale vortical structure with cyclonic (positive) vertical vorticity that extends over the domain height. The vortex is embedded in an environment with weak anticyclonic (negative) vorticity. Remarkably, L52NS [Fig. 3(c)] displays both a cyclonic and an anticyclonic vortex. Just as the vortex monopole, the dipole spans the domain height. During the statistically stationary state [approximately 400 (900) convective times H/U_{ff} at $\text{Pr} = 0.1$ (5.2)], the vortices are long-lived without significant horizontal displacement. For P52NS [Fig. 3(d)], plumes dominate the bulk [4,9,30].

Cyclonic vortices are favored over anticyclones: when both are present, the anticyclone is weaker than the cyclone. Cyclone-anticyclone asymmetry in rotating flows has been extensively discussed [31–34], also in vortex condensates [35].

To study the development of LSVs, we consider the shell-to-shell energy transfer [11,37,38]. We investigate [10] transfer from baroclinic to barotropic (3D to 2D) flow:

$$T_{\text{bc}}(Q, K) \equiv - \int_V \langle \mathbf{u}_K \rangle_z \cdot (\mathbf{u}' \cdot \nabla) \mathbf{u}'_Q dV, \quad (1a)$$

and barotropic self-interaction (2D to 2D):

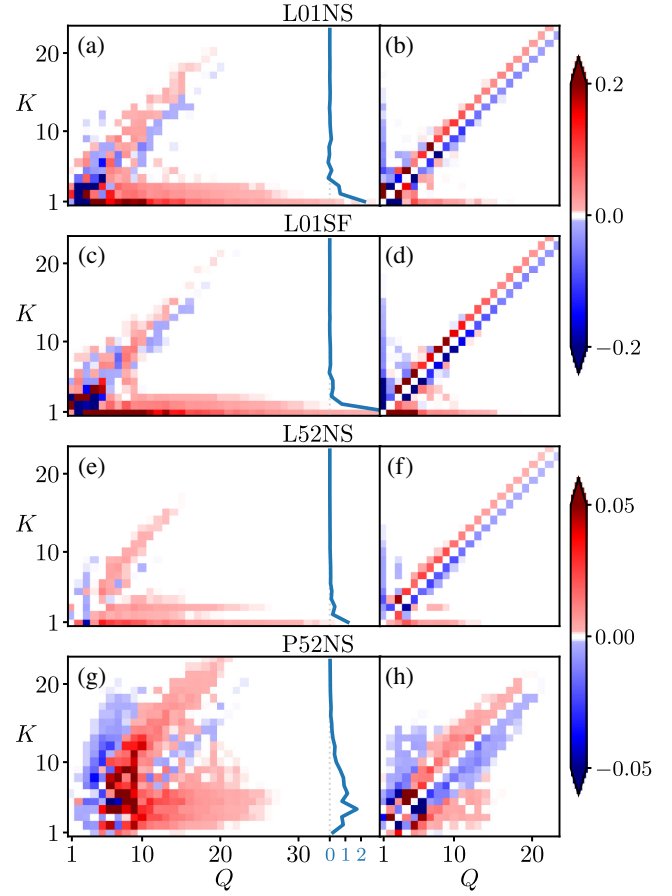


FIG. 4. Spectral kinetic energy transfer T_{bc} from (baroclinic) 3D mode Q to (barotropic) 2D mode K [panels (a), (c), (e), (g)] and T_{bt} between (barotropic) 2D modes Q and K [panels (b), (d), (f), (h)], normalized by mean buoyant energy input $\langle w\theta \rangle_V$, for the reference cases (a),(b) L01NS, (c),(d) L01SF, (e),(f) L52NS and (g),(h) P52NS. Blue curves represent $T_{\text{bc}}^{\geq 5}(K)$.

$$T_{\text{bt}}(Q, K) \equiv - \int_V \langle \mathbf{u}_K \rangle_z \cdot (\langle \mathbf{u} \rangle_z \cdot \nabla) \langle \mathbf{u}_Q \rangle_z dV. \quad (1b)$$

The Fourier-filtered 2D field $\langle \mathbf{u}_K \rangle_z$ of wave number K receives energy from the filtered (2D or 3D) field of wave number Q via triadic interactions mediated by the energy giver field; we find that the other transfers to 2D (from 3D mediated by 2D and from 2D mediated by 3D) are negligible. If $T_{\text{bc}}, T_{\text{bt}} > 0$, the mode Q transfers energy to mode K and vice versa. Equations (1a) and (1b) are derived from the budget equation of modal barotropic kinetic energy, where Fourier transforms are performed in the horizontal periodic directions and the Fourier space divided into ringlike shells of different horizontal wave numbers.

In Fig. 4 we plot T_{bc} (left column) and T_{bt} (right column). LSV cases (top three rows) present positive T_{bc} over a wide range of modes $Q \gtrsim 5$ and $K \lesssim 3$, revealing spectrally *nonlocal* upscale transfer of kinetic energy from 3D convection at small scales to the largest 2D scales, i.e.,

without participation of intermediate scales. We also plot $T_{bc}^{\geq 5}(K) \equiv \sum_{Q=5}^{40} T_{bc}(Q, K) / \langle w\theta \rangle_V$ (blue curves), the sum of nonlocal baroclinic transport to mode K , normalized by volume-averaged buoyant energy input $\langle w\theta \rangle_V$ (θ is temperature). The largest contribution is indeed at LSV mode $K = 1$.

For plumes [Fig. 4(g)], a narrower range of baroclinic modes $5 \lesssim Q \lesssim 25$ contributes positively to barotropic modes $2 \lesssim K \lesssim 10$, with virtually no contribution to $K = 1$. We argue that this upscale energy transfer is due to plume-plume interactions and merger (plume scale is $K_p \approx 10$); spectrally local unlike the strong interaction of all Q with $K = 1$ in LSV cases, together with a direct downscale cascade.

In all cases T_{bt} presents positive diagonal $K = Q + 1$, indicating spectrally *local* downscale transfer within the 2D flow. Additionally, LSV cases reveal spectrally non-local upscale transfer: positive T_{bt} at $K = 1$ over a wide range of Q modes (likewise, negative T_{bt} for $Q = 1$). Simultaneous downscale and upscale transfers coexist within the 2D flow [10]. Finally, for P52NS [Fig. 3(d)], some 2D self-interaction is registered: energy exchanges among plumes lead to short-range upscale transfer toward scales that do not involve the largest scale, with concurrent downscale cascades over a much shorter range than for LSVs.

To investigate the near-wall dynamics, we calculate the (nondimensional) height-dependent planar kinetic energy budget [39–41]:

$$\mathcal{B} + \mathcal{T} + \mathcal{P} + \mathcal{V} - \mathcal{D} = 0, \quad (2)$$

where $\mathcal{B} \equiv \langle w\theta \rangle_P$ is buoyant production, $\mathcal{T} \equiv -\partial_z \langle wE_t \rangle_P$ turbulent transport, $\mathcal{P} \equiv -\partial_z \langle wp \rangle_P$ pressure transport, $\mathcal{V} \equiv 2\sqrt{\text{Pr}/\text{Ra}} \partial_z \langle u_i s_{i3} \rangle_P$ viscous transport, and $\mathcal{D} \equiv \langle \epsilon \rangle_P = 2\sqrt{\text{Pr}/\text{Ra}} \langle s_{ij} s_{ij} \rangle_P$ dissipation rate [42]. $\langle \dots \rangle_P$ denotes horizontal planar averaging, p is pressure, and $s_{ij} = \frac{1}{2}(\partial_j u_i + \partial_i u_j)$. Summation is over repeated indices, $i = 1, 2$ denote horizontal directions and $i = 3$ vertical direction ($u_3 = w$). We normalize all terms with $\langle w\theta \rangle_V$. \mathcal{B} indicates energy input; transport terms (\mathcal{T} , \mathcal{P} , \mathcal{V}) redistribute kinetic energy vertically; \mathcal{D} extracts energy.

Figure 5 shows the z -dependent budgets for the reference cases; left column for lower half of the domain, right column zoomed in on the bottom BL. For all cases, \mathcal{B} provides energy in the bulk. For L01SF, this energy input is nicely balanced by dissipation, i.e., $\mathcal{D} \approx \mathcal{B}$, whereas $\mathcal{D} < \mathcal{B}$ for no-slip cases. There, \mathcal{B} is compensated by large \mathcal{D} near the walls, as $z/\delta_\nu \rightarrow 0$. The difference between \mathcal{B} and \mathcal{D} in the bulk is redistributed toward the BLs by \mathcal{P} ; the other two transport terms are marginal and only participate near the walls. For LSVs, this extraction may slightly reduce the amount of energy available for interscale exchanges, but does not prevent its spectral transfer upscale. To emphasize this, we co-plot

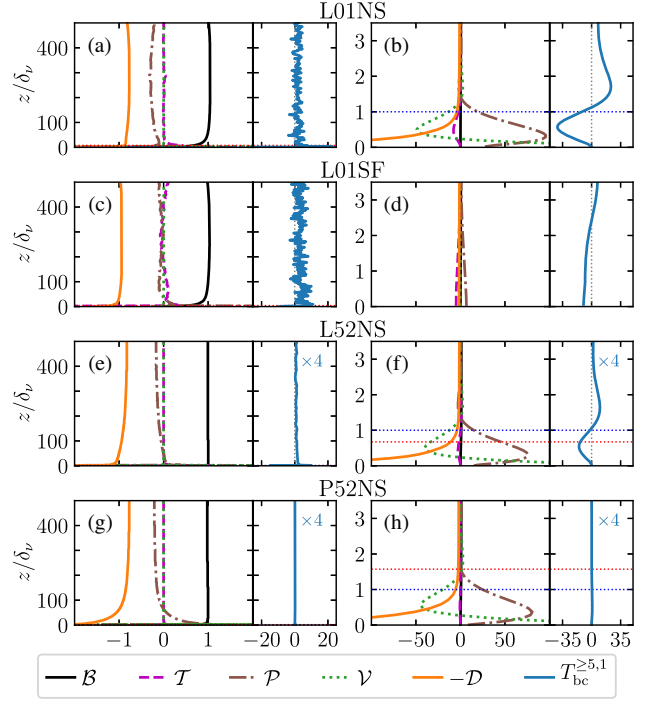


FIG. 5. Kinetic energy budget in the bulk [panels (a), (c), (e), (g)] and near the bottom [panels (b), (d), (f), (h)] for the reference cases (a),(b) L01NS, (c),(d) L01SF, (e),(f) L52NS and (g),(h) P52NS. Vertical coordinate scaled by viscous BL thickness δ_ν (for L01SF we use δ_ν from L01NS). Profiles shown for lower half of the domain; midheight $z/\delta_\nu \approx 400$ for all cases. Dotted blue (red) horizontal lines denote viscous (thermal) BL thicknesses. The thermal BL is thicker than the plotting interval in (b),(d). Blue curves indicate height-dependent nonlocal energy transfer $T_{bc}^{\geq 5,1}(z)$ from 3D modes $5 \leq Q \leq 40$ to 2D LSV mode $K = 1$.

with blue curves the height-dependent transfer to 2D mode $K = 1$, $T_{bc}^{\geq 5,1}(z) \equiv \sum_{Q=5}^{40} T_{bc}(Q, K = 1, z) / \langle w\theta \rangle_V$. We find predominantly positive $T_{bc}^{\geq 5,1}$ throughout the bulk for LSVs, and vanishingly small $T_{bc}^{\geq 5,1}(z)$ where no large scales develop.

Near the no-slip walls [Figs. 5(b), 5(f), 5(h)], the budget resembles that of rotationally constrained flows [41]: pressure transport supplies energy to sustain the Ekman BL against frictional dissipation [1], viscous transport redistributes energy within the BL, while turbulent transport has little to no contribution to the budget. Notably, for LSVs [Figs. 5(b) and 5(f)], no 3D-to-2D upscale transfer is sustained within the BL: $T_{bc}^{\geq 5,1} < 0$ for $z < \delta_\nu$. Instead, the 2D mode loses energy to smaller-scale 3D motions. $T_{bc}^{\geq 5,1} > 0$ for $z > \delta_\nu$ and, strikingly, it peaks just outside the BL to reduce (but remain positive) toward the bulk. As vertical bursts from the BL [$w_{\text{KURT}} > 3$ at $z = \delta_\nu$, see Fig. 2] are sheared apart by the strong horizontal bulk flow, their energy feeds the upscale transfer to the 2D LSV just outside the BL. The thermal BL has no noticeable effect on these profiles.

We demonstrate that Ekman BLs cannot prohibit LSV formation in no-slip RRBC. They, instead, postpone the occurrence of upscale energy transfers to significantly higher rotation rates (at the same supercriticality) than for stress-free boundaries; vertical bursts due to Ekman pumping require stronger rotational constraint to be diverted into upscale transfer to LSVs. Ekman plumes are swept away by large horizontal velocities from the emerging LSVs. The role of the Prandtl number is similar for no-slip as for stress-free simulations: LSV formation is more easily reached at smaller Pr [9]. We postulate that coherent plumes, formed by the Ekman BLs, with strong temperature contrast, are longer lived at high Pr given weaker thermal diffusion. Hence they can more proficiently disturb LSV formation.

Large-scale flow organization is ubiquitous in geophysics and astrophysics. Our study identifies that Ekman boundary layers are unable to prevent vortex condensation, opening up laboratory modeling of these flows in the rotating Rayleigh-Bénard configuration [43]. We provide firm evidence that large-scale vortex condensation can develop regardless of the boundary conditions.

A. J. A. G., M. M., J. S. C., and R. P. J. K. received funding from the European Research Council (ERC) under the European Union's Horizon 2020 research and innovation programme (Grant Agreement No. 678634). We are grateful for the support of the Netherlands Organisation for Scientific Research (NWO) for the use of supercomputer facilities (Cartesius) under Grants No. 15462, No. 16467, and No. 2019.005. Volume renders are produced using VAPOR [44], a product of the Computational Information Systems Laboratory at the National Center for Atmospheric Research.

*Present address: Department of Mechanical Engineering, University of Rochester, Rochester, New York 14623, USA.
†r.p.j.kunnen@tue.nl

- [1] J. Pedlosky, *Geophysical Fluid Dynamics* (Springer, New York, 1979).
- [2] S. Sakai, *J. Fluid Mech.* **333**, 85 (1997).
- [3] P. Vorobieff and R. E. Ecke, *J. Fluid Mech.* **458**, 191 (2002).
- [4] R. P. J. Kunnen, H. J. H. Clercx, and B. J. Geurts, *Phys. Rev. E* **82**, 036306 (2010).
- [5] S. Stellmach, M. Lischper, K. Julien, G. Vasil, J. S. Cheng, A. Ribeiro, E. M. King, and J. M. Aurnou, *Phys. Rev. Lett.* **113**, 254501 (2014).
- [6] K. M. J. Alards, R. P. J. Kunnen, R. J. A. M. Stevens, D. Lohse, F. Toschi, and H. J. H. Clercx, *Phys. Rev. Fluids* **4**, 074601 (2019).
- [7] G. Ahlers, S. Grossmann, and D. Lohse, *Rev. Mod. Phys.* **81**, 503 (2009).
- [8] R. J. A. M. Stevens, H. J. H. Clercx, and D. Lohse, *Phys. Fluids* **23**, 095110 (2011).
- [9] K. Julien, A. M. Rubio, I. Grooms, and E. Knobloch, *Geophys. Astrophys. Fluid Dyn.* **106**, 392 (2012).
- [10] A. M. Rubio, K. Julien, E. Knobloch, and J. B. Weiss, *Phys. Rev. Lett.* **112**, 144501 (2014).
- [11] B. Favier, L. J. Silvers, and M. R. E. Proctor, *Phys. Fluids* **26**, 096605 (2014).
- [12] C. Guervilly, D. W. Hughes, and C. A. Jones, *J. Fluid Mech.* **758**, 407 (2014).
- [13] R. P. J. Kunnen, R. Ostilla-Mónico, E. P. Van Der Poel, R. Verzicco, and D. Lohse, *J. Fluid Mech.* **799**, 413 (2016).
- [14] R. H. Kraichnan, *Phys. Fluids* **10**, 1417 (1967).
- [15] G. K. Batchelor, *Phys. Fluids* **12**, II (1969).
- [16] L. M. Smith and V. Yakhot, *J. Fluid Mech.* **274**, 115 (1994).
- [17] M. Chertkov, C. Connaughton, I. Kolokolov, and V. Lebedev, *Phys. Rev. Lett.* **99**, 084501 (2007).
- [18] A. Frishman and C. Herbert, *Phys. Rev. Lett.* **120**, 204505 (2018).
- [19] G. Boffetta and R. E. Ecke, *Annu. Rev. Fluid Mech.* **44**, 427 (2012).
- [20] A. Alexakis and L. Biferale, *Phys. Rep.* **767**, 1 (2018).
- [21] K. Julien, J. M. Aurnou, M. A. Calkins, E. Knobloch, P. Marti, S. Stellmach, and G. M. Vasil, *J. Fluid Mech.* **798**, 50 (2016).
- [22] M. Plumley, K. Julien, P. Marti, and S. Stellmach, *J. Fluid Mech.* **803**, 51 (2016).
- [23] S. Chandrasekhar, *Hydrodynamic and Hydromagnetic Stability* (Oxford University Press, New York, 1961).
- [24] J. M. Aurnou, V. Bertin, A. M. Grannan, S. Horn, and T. Vogt, *J. Fluid Mech.* **846**, 846 (2018).
- [25] R. Ostilla-Mónico, Y. Yang, E. P. van der Poel, D. Lohse, and R. Verzicco, *J. Comput. Phys.* **301**, 308 (2015).
- [26] Relatively wider domains are simulated at $Pr \approx 5$ thanks to the multiple-resolution approach.
- [27] J. S. Cheng, S. Stellmach, A. Ribeiro, A. Grannan, E. M. King, and J. M. Aurnou, *Geophys. J. Int.* **201**, 1 (2015).
- [28] D. Nieves, A. M. Rubio, and K. Julien, *Phys. Fluids* **26**, 086602 (2014).
- [29] H. Xia, D. Byrne, G. Falkovich, and M. Shats, *Nat. Phys.* **7**, 321 (2011).
- [30] R. P. J. Kunnen, B. J. Geurts, and H. J. H. Clercx, *J. Fluid Mech.* **642**, 445 (2010).
- [31] E. J. Hopfinger, F. K. Browand, and Y. Gagne, *J. Fluid Mech.* **125**, 505 (1982).
- [32] C. N. Baroud, B. B. Plapp, H. L. Swinney, and Z.-S. She, *Phys. Fluids* **15**, 2091 (2003).
- [33] B. Sreenivasan and P. A. Davidson, *Phys. Fluids* **20**, 085104 (2008).
- [34] F. S. Godeferd and F. Moisy, *Appl. Mech. Rev.* **67**, 030802 (2015).
- [35] In Ref. [36] the presence or absence of the anticyclone is postulated to result from either of two saturation mechanisms: one due to viscous forces, as in 2D turbulence, and another independent of viscosity reliant on the breaking of Q2D conditions in the rotating flow.
- [36] K. Seshasayanan and A. Alexakis, *J. Fluid Mech.* **841**, 434 (2018).
- [37] A. Alexakis, P. D. Mininni, and A. Pouquet, *Phys. Rev. E* **72**, 046301 (2005).
- [38] P. D. Mininni, A. Alexakis, and A. Pouquet, *Phys. Fluids* **21**, 015108 (2009).

- [39] J. W. Deardorff and G. E. Willis, *J. Fluid Mech.* **28**, 675 (1967).
- [40] R. M. Kerr, *Phys. Rev. Lett.* **87**, 244502 (2001).
- [41] R. P. J. Kunnen, B. J. Geurts, and H. J. H. Clercx, *Eur. J. Mech. B* **28**, 578 (2009).
- [42] S. B. Pope, *Turbulent Flows* (Cambridge University Press, Cambridge, England, 2000).
- [43] J. S. Cheng, J. M. Aurnou, K. Julien, and R. P. J. Kunnen, *Geophys. Astrophys. Fluid Dyn.* **112**, 277 (2018).
- [44] www.vapor.ucar.edu.